A kinetic study of methane partial oxidation over FeZSM-5 using N_2O as an oxidant

Ying Kit Chow[a], Nicholas F. Dummer[a]*, James H. Carter[a], Randall J. Meyer[b], Robert D. Armstrong[a], Christopher Williams[a], Greg Shaw[a], Sara Yacob[b], Madan M. Bhasin[c], David J. Willock[a], Stuart H. Taylor[a], and Graham J. Hutchings[a]*

[a] Cardiff Catalysis Institute, School of chemistry, Cardiff University, Main Building, Park Place, Cardiff, CF10 3AT, UK.

[b] ExxonMobil Research and Engineering, Corporate Strategic Research, Annandale, NJ 08801, USA

[c] Innovative Catalytic Solutions, LLC, Charleston, WV, 25314, USA.

* Corresponding author emails: dummernf@cardiff.ac.uk and hutch@cardiff.ac.uk

Abstract

Catalytic methane oxidation using N_2O was investigated at 300 °C over Fe-ZSM-5. This reaction rapidly produces coke (retained organic species), and causes catalyst fouling. The introduction of water into the feed-stream resulted in a significant decrease in the coke selectivity and an increase in the selectivity to the desired product, methanol, from *ca.* 1 % up to 16 %. A detailed investigation was carried out to determine the fundamental effect of water on the reaction pathway and catalyst stability. The delplot technique was utilised to identify primary and secondary reaction products. This kinetic study suggests that observed gas phase products; CO, CO_2, CH_3OH, C_2H_4 and C_2H_6 form as primary products whilst coke is a secondary product. Dimethyl ether was not detected, however we consider that the formation of C_2 products are likely to be due to an initial condensation of methanol within the pores of the zeolite and hence considered pseudo-primary products. According to a second order delplot analysis, coke is considered a secondary product and its formation correlates with CH_3OH formation. Control experiments in the absence of methane revealed that the rate of N_2O decomposition is similar to that of the full reaction mixture, indicating that the loss of active *alpha*-oxygen sites is the likely cause of the decrease in activity observed and water does not inhibit this process.

Keywords; MFI zeolite, methane oxidation, delplot, methanol, Fe-ZSM-5.

Introduction

Methanol is currently produced from methane industrially by an energy-intensive two-step process involving high-temperature reforming, followed by methanol synthesis.[1-4] The direct oxidation of methane to methanol could provide economic benefits for industries and a decentralised process would offer an environmentally conscious alternative to methane flaring.[5] However, this reaction remains a scientific and technical challenge due to the low reactivity of methane and limited methanol selectivity observed when using oxides or supported metal catalysts.[6]

Recently, a number of zeolite-based systems have been reported which provide an alternative approach to partial methane oxidation.[7-10] Tomkins *et al.* reported an isothermal catalytic cycle, converting methane into methanol over Cu-mordenite.[11] In this process the catalyst is first activated using molecular oxygen, followed by reaction with methane. Methanol was subsequently extracted using steam, to clear the active site for further oxidation cycles. Roman-Leshkov and co-workers have shown that continuous catalytic production of methanol from oxygen, water and methane can be achieved with copper zeolites if the process conditions are carefully chosen.[7] Cu- containing zeolites were also utilised by Sushkevich *et al*., who reported direct, partial oxidation to methanol using water as both solvent and oxygen source.[12] Use of water in this anaerobic methane oxidation system indicated that water could act as a cheap oxidant in methane oxidation. Furthermore, water served as an agent in regenerating the active site through facilitating desorption of partially oxygenated products.[12] In contrast to the above systems, it has been shown that using H_2O_2[13] or N_2O[14] as the primary oxidant, higher conversions in a continuous process can be achieved. Panov and co-workers[14] reported gas-phase methane oxidation under a catalytic regime using an α-oxygen species generated when Fe-ZSM-5 was treated with N_2O at 300 °C, and methanol was formed under a continuous flow regime. The α-oxygen was generated by decomposing N_2O over the reversible redox α-Fe sites, which switch from Fe^{2+} to Fe^{3+}.[14, 15] The exact structure of the oxygen transition state remains debatable however, and is generally thought to comprise a mononuclear Fe^{4+}=O or $(Fe^{3+}\text{-}O^{-})_{\alpha}$ site.[15, 16] Catalyst deactivation was observed and this was attributed to appreciable coke formation, which led to catalyst fouling. The same group later reported that addition of water into the feed-stream significantly improved both the carbon balance and methanol selectivity, with the latter increasing from 1.9 % to 19 % when 20 % v/v steam was added.[14] Co-feeding of water with the N_2O and methane also increased the selectivity to CO.[14, 17] Furthermore, the effect of water has been shown to effect the decomposition of N_2O through hydroxylation of the $(Fe^{3+}\text{–}O^{-})_{\alpha}$ sites to form $(Fe^{3+}\text{–}OH^{-})_{\alpha}$ which requires temperatures above 400 °C to reactivate the α-Fe sites.[15] Similarly, Bulushev *et al*. demonstrated the

effect of co-fed water on N_2O decomposition over Fe-ZSM-5 and indicated that N_2O reversible adsorption, $(O)_{Fe}$ loading from N_2O and O_2 desorption were affected.[18]

The reaction mechanism of CH_4 oxidation using N_2O over Fe-ZSM-5 is complex and involves parallel reaction pathways, which are not fully understood. The delplot technique, first developed by Bhore *et al*., is a powerful tool for determining the rank of reaction products, where multiple pathways occur simultaneously.[19] The method uses a plot of molar yield/conversion versus conversion and aids the identification of primary and non-primary reaction products. For example, Wei *et al*. employed the delplot method in their analysis of the selective hydrogenation of acrolein on supported silver catalysts[20] and found that while the desired product allyl alcohol was a primary product, propanal was both a primary product and a secondary product, via isomerisation of allyl alcohol. Rajkhowa *et al*. applied the technique in a kinetic study of Cu- catalysed liquid phase glycerol hydrogenolysis [21]. Using delplot analysis, the authors were able to identify that acetol was the primary product and propylene glycol was a secondary product.[21]

In the present work, we investigate the effect of water addition to the feed on the oxidation of methane using N_2O over Fe-ZSM-5. Specifically, we apply the delplot technique to investigate the way in which water addition affects reaction pathways. We then study the mechanism by which catalyst deactivation occurs, through characterisation of catalysts both prior to and following catalytic testing. Comparison of the pre- and post-reaction catalyst samples indicate that H_2O can prevent Fe migration along with reduced coking, although N_2O conversion was found to decrease at a similar rate in both systems. These findings highlight the complex nature of the methane oxidation reaction over Fe-ZSM-5 catalysts.

Experimental

Preparation of H-ZSM-5

NH_4-ZSM-5 (Zeolyst, SiO_2:Al_2O_3 molar ratio = 30, 3 g) was calcined under flowing air at 550 °C, with a temperature ramp of 20 °C min^{-1} for 3h to yield H-ZSM-5 (30). The sample was then allowed to cool to room temperature under flowing air.

Preparation of Fe-ZSM-5

All catalysts were prepared by chemical vapour impregnation (CVI). H-ZSM-5 (30) (1.98 g) and Fe (III) acetylacetonate ($Fe(acac)_3$) (Sigma Aldrich, 99.9% purity, 2.53 g) were physically mixed and then heated to 150 °C under continuous vacuum (*ca* 10^{-3} mbar) for 2 h. The resulting material was allowed to cool to room temperature prior to calcination in static air for 3 h (550 °C, temperature ramp at 20 °C min^{-1}). The Fe-ZSM-5 was pelleted to a mesh size of 20-40 prior to testing.

Catalyst Testing

Methane oxidation reactions were performed in a fixed bed continuous flow reactor. The desired mass of catalyst (typically 0.44 g and from 0.12 to 1.2 g to construct the delplot) was placed in a stainless steel tube supported by quartz wool. In a typical methane oxidation reaction the feed mixture comprised of 20 % CH_4 (Air Products) + 2 % N_2O (BOC, AA Grade) with Ar (BOC Pureshield) balance (total flow rate = 55 ml min^{-1}, typically GHSV = 3600 h^{-1}) at 1 atm pressure. The reaction temperature (typically 300 °C) was controlled by an isothermal oven (± 1 °C) with a thermocouple located directly above the catalyst bed.

The addition of water to the reaction stream was carried out using a syringe pump (Sono-Tek, Syringe Pump TI). The total flow rate of the feed mixture in the presence of water was kept at 55 ml min^{-1}, containing 20 % CH_4 + 20 % H_2O + 2% N_2O (Ar balance). Post-reaction catalyst samples will be referred to as (i) Fe-ZSM-5-0% (no water added to feed stream) and (ii) Fe-ZSM-5-20% (20 % v/v water added to the feed-stream).

Reaction products were analysed with online gas chromatography (GC) at 30 min intervals using an Agilent 7890B GC equipped with a methaniser. CH_4, CO, CO_2, C_2H_4 and C_2H_6 were detected and quantified by flame ionisation detector (FID) using a Hayesep packed column. Methanol, dimethyl ether and aromatic products were detected by FID following separation on a capillary column (Agilent, PoraBOND U). N_2O and N_2 were detected by a thermal conductivity detector (TCD).

CH_4 and N_2O conversions were calculated according to Equations 1 and 2.

$$\mathrm{CH_4\ conversion\ (\%)} = \frac{\mathrm{CH_4}_{\ in} - \mathrm{CH_4}_{\ out}}{\mathrm{CH_4}_{\ in}} \times 100 \qquad \text{Equation 1}$$

where, $CH_{4\ in}$ and $CH_{4\ out}$ represent the molar fraction of CH_4 at the inlet and outlet, respectively.

$$\mathrm{N_2O\ conversion\ (\%)} = \frac{\mathrm{N_2O_{in}} - \mathrm{N_2O_{out}}}{\mathrm{N_2O_{in}}} \times 100 \qquad \text{Equation 2}$$

Where, N_2O_{in} and N_2O_{out} represent the molar fraction of N_2O at the inlet and outlet, respectively.

The selectivity for product (S_i) was calculated as follows, coke assumed to be the remainder:

$$S_i\ (\%) = \frac{\mathrm{amount\ of\ product\ (i)\ produced\ \ (mol\ carbon)}}{\mathrm{CH_4\ converted\ (mol\ carbon)}} \times 100 \qquad \text{Equation 3}$$

Catalyst characterisation

Diffuse-reflectance UV-Vis spectra were collected using an Agilent Cary 4000 UV-vis spectrophotometer. Samples were scanned between 200 and 800 nm (400 nm min^{-1}). Thermal gravimetric analysis (TGA) was performed using a PerkinElmer TGA 4000. Samples (*ca*. 20 – 30 mg) were loaded into ceramic crucibles and then heated to 900 °C (5 °C min^{-1}) under a flow of air (50 ml min^{-1}). Nitrogen adsorption isotherms were collected on a Micromeritics 3Flex. Samples (*ca*. 0.020 g) were degassed (150 °C, 6 h) prior to analysis. Analyses were carried out at -196 °C with P_0 measured continuously. Free space was measured post- analysis with He. Pore size analysis was carried out using Micromeritics 3Flex software, N_2-Cylindrical Pores- Oxide Surface DFT Model.

Results and discussion

Catalytic reactions

Methane oxidation reactions were conducted over Fe-ZSM-5 catalysts in the presence of N_2O and where reported, co-fed H_2O. This catalyst was extensively characterised in our previous report[22] in an effort to deconvolute the influence of the Fe location and framework acidity on CH_4 oxidation with N_2O. Figure 1a shows the product distribution of 2 % Fe-ZSM-5 catalysed methane oxidation with increasing time-on-stream and Figure 1b shows methane conversion, N_2O conversion and carbon balance values for the same reaction, which was carried out in the absence of added water vapour. Catalytic oxidation of methane with N_2O is observed over Fe-ZSM-5,[14, 23-25] with low selectivity towards methanol of *ca.* 1 %. Parfenov *et al*.[14] reported that addition of water to the feed-stream can improve methanol selectivity whilst also inhibiting the accumulation of coke and retained organics. Trends are consistent with those observed by Parfenov *et al*. who reported decreasing rates of methane and N_2O conversion over the initial 100 min on stream. This is consistent with the gradual decrease in detected carbonaceous products observed in Figure 1b at longer times-on-stream. Similarly, CO selectivity decreases from *ca.* 60 % to 16 %, whilst selectivity towards C_2 products increases from 0.6 % to 4.4 % over the same period. Selectivities towards methanol and CO_2 (1.4 % and 12 % selectivity respectively) are constant over the 2.5 h testing period. Interestingly, no DME or acetaldehyde were detected in the reactor effluent.

With an aim to suppress catalyst fouling and be consistent with the approach taken by Parfenov *et al*. water vapour (20 % v/v) was introduced into the feed stream and results are shown in Figure 2. A significant increase in methanol selectivity is observed relative to the water- free system, from 1.4 % to 16 %. A corresponding increase in mass balance is also observed in Figure 2, with less than 30 % of the methane conversion lost to coke. It has previously been reported that water promotes hydroxylation and facilitates desorption of methanol from the catalyst surface.[26] The formation of methanol is associated with *alpha*-oxygen, which is generated by decomposition of N_2O on Fe.[27-29] However, due to the structure of the ZSM-5 zeolite, CH_3OH has been observed to react at Brønsted acidic sites to yield DME and higher hydrocarbons.[22, 30] This may be alleviated by removing or blocking Brønsted acid sites and thereby improve CH_3OH selectivity and carbon mass balance. Furthermore, these findings strongly imply that Brønsted acidity facilitates the conversion of DME into ethene and eventually, coke.[22, 30, 31]

It is clear that the addition of water leads to a significant improvement in methanol selectivity and the yield at 1.5 h time-on-stream is 0.16 % (without H_2O the yield is 0.02 %). This might be assigned to

water facilitating methanol desorption and competitively adsorbing at Brønsted acid sites.[15, 32] A further benefit is the reduction in the concentration of C_2 products, specifically C_2H_6, which is absent from the reaction effluent. We consider that C_2H_6 is formed from C_2H_4, probably via methyl benzenes, through the hydrocarbon pool mechanism.[22, 33, 34] Accordingly, water has decreased the effective Brønsted acidity of the zeolite surface and thereby limiting C_2H_6 formation. This observation is consistent with the recent reports of White and co-workers[32] who studied the effect of water on Brønsted acid sites by measuring C-H activation over H-ZSM-5. They reported that at higher water concentrations (> 2-3 molecules of water per Brønsted acid site) water inhibited the rate of isobutene activation. We consider that 20 % water in the feed stream is sufficiently high to induce the previously observed inhibition of Brønsted acidity. Interestingly, the CO_2 selectivity remains at *ca.* 12 % independent of feed composition (i.e. water/ no water). This implies that CO_2 forms directly from methane at Fe sites, as we previously reported low selectivity towards CO_2 (< 1 %) when methanol and N_2O was passed over H-ZSM-5, Fe-ZSM-5, Fe-TS-1 or Fe-Silicalite.[22] Therefore, it is reasonable to postulate that methane can be oxidised to CO_2 via a second pathway and not exclusively via oxidation of CO (Scheme 1). Indeed, Parfenov *et al*.[14] reported that the majority of CO is formed through the decomposition of formic acid, itself formed through the disproportionation of formaldehyde, a short-lived reaction intermediate not via combustion of CH_4.

Figure 2b shows that following an initial stabilization period, methane conversion reaches a steady state at 1.1 %. Across the same period, a more pronounced decrease in N_2O conversion is observed. Indeed, decreasing N_2O conversion is observed in both Figs. 1 and 2. To compare the systems represented in Figures 1 and 2, both methane and N_2O conversion were normalised to their initial value, and plotted as a function of time (Fig. 3). A clear decrease in conversion is observed over the 3 h testing period. Notably, this deactivation is insensitive to the presence/ absence of water in the substrate feed (Fig. 3). This implies that the deactivation mechanism is not solely related to the blocking of active sites through coke formation (Fig. 1 and 2). This is in contrast to studies by Panov and co-workers, who observed that the addition of water stabilised conversion over 2 h on line.

To further study the effect of water addition upon reaction pathways during Fe-ZSM-5 catalysed methane oxidation, the delplot technique was applied. The delplot technique, first developed by Bhore *et al*., assists in resolving the rank of products where multiple, simultaneous reaction pathways occur.[19] This is achieved firstly through plotting of selectivity versus conversion and then by plotting selectivity/conversion versus conversion or selectivity/conversion^2 versus conversion and allows primary, secondary and higher rank products respectively to be identified independent of reaction

order. Through extrapolation to zero conversion, primary products can be identified where the intercepts are finite in the first plot and then asymptotic for the second and third plots.

Methane and N_2O were passed over 2 wt.% Fe-ZSM-5 in a series of experiments using various catalyst masses, whilst the total bed volume was kept constant through addition of SiC fines. This afforded a conversion profile and enabled assessment of product orders through a delplot (Fig. 4, for minor product plots see supplemental information Fig. S1). The methane conversion used in this analysis ranged from *ca.* 0.4 to 3.1 %. In general, at low conversion conditions the loss of carbon is 30 % of the total converted carbon and the products detected in the GC are ranked according to their selectivity in the following order: $CO > CO_2 > C_2H_4 > C_2H_6 \geq CH_3OH$. As the conversion of methane increases, the mass balance decreases significantly, *i.e.* the selectivity to coke or retained organics increases and selectivity towards gas phase products decreases. The delplot analysis would therefore suggest that coke is a secondary product and the remaining products are primary (Fig. 4 b). Interestingly, analysis of the data presented in the third-rank delplot in Figure 4c suggests that the missing carbon or coke is not a higher or tertiary ranked product as the line of best fit is asymptotic. That is, extrapolation of the line of best fit to the origin indicates that first rank plots for CH_3OH, CO, CO_2, C_2H_4 and C_2H_6 would not pass through the origin (see Fig. S1). Clearly, the presence of a C_2 product in the reaction effluent implies coupling of C_1 products and thereby C_2 products could be classed as secondary products. Furthermore, C_2H_6 selectivity increases over the initial 100 min on-line, both in the presence and absence of co-fed H_2O (Fig. 1 and 2). However, the delplot in Figure 4 is constructed from data at times of > 100 min, once steady state of CH_4 conversion is observed and therefore this is not fully captured. According to a reaction mechanism proposed by Panov and co-workers[14, 25, 35] methanol and/or formaldehyde are the primary product(s) of methane oxidation. Methanol might then desorb into the gas phase or transfer to other surface sites on Fe-ZSM-5 to eventually form coke via a surface bound ether (DME). We consider that C_2H_6 desorbs from these surface bound ether species in a comparable mechanism to that found in MTO chemistry.[36] The high concentration of coke in this reaction appears to support the conclusions expressed by Panov and co-workers with respect to the beneficial effect of water displacing CH_3OH more efficiently. The delplot data obtained with Fe-ZSM-5-0% indicates that, as methane conversion increases, coke formation comes to dominate the product distribution. The formation of coke as opposed to combustion products in this case implies that the reaction is either oxidant limited or that the strength of product adsorption is higher than that of methane.

Figure 5a-c illustrates the pathway analysis of the reaction of methane and N_2O over 2 % Fe-ZSM-5 where 20 % v/v water is present in the feed-stream (for minor product plots see Fig. S2). The reaction was studied over a conversion range of 0.7 to 2.3 %. Clearly, the formation of coke is greatly reduced

even at higher conversion values, as noted in the analysis of the time-on-line data (Fig. 2). Both CH_3OH and CO selectivities are enhanced across the conversion range, which further indicates the importance of water in the formation of CO and CH_3OH.[14] At low conversion (< 1 %) the selectivity to CH_3OH and coke are less when combined at *ca*. 35 % than the selectivity to CO at 55 % (Fig. 5a). We consider that the coke formation is most likely due to retention of CH_3OH or a methoxy species. Indeed, if all the CH_3OH produced under these conditions could be desorbed then the CH_3OH : CO ratio would be less than 1:1, as was observed by Panov and co-workers.[14] Therefore, the formation of CO cannot solely be due to the decomposition of HCOOH formed from the disproportionation of HCHO. With increasing conversion, this ratio is disrupted significantly; the selectivity of CO at a conversion of 2.5 %, is 30 % and that of CH_3OH is 10 %, whereas coke is 55 %. Under these reaction conditions, water is less able to promote CH_3OH desorption and so sufficient methanol builds up to allow coke formation. Figure 5b illustrates the second-rank delplots from this data set which suggests that coke is a secondary product as the intercept is no longer close to the origin. Had the line of best fit extrapolated to the origin in the second-rank delplot, coke could be considered a higher order product. In contrast to Fig. 4c, that shows coke to exponentially increase as the conversion decreases (confirming it as a secondary product), the presence of water results in a more linear regression to the y axis intercept in Fig. 5c, suggesting that the kinetic pathway has been altered. Specifically, the formation of coke in the presence of water appears to also be a tertiary product. This can be interpreted as the result of the reduction in the rate of coke formation. Interestingly, the selectivity of CO_2 (*ca.* 10 %) (Fig. 5a) does not alter substantially across the conversion range studied, implying an independent pathway to that of CO and CH_3OH. Furthermore, C_2H_6 is not detected in the reaction effluent, which suggests that water can prevent readsorption of C_2H_4.

Based on these data, we consider that water has a beneficial effect at low conversion conditions (<1 %), however, at higher conversion (> 1%) it appears unable to competitively adsorb and displace CH_3OH as effectively. Indeed, Hunger *et al*. observed that methanol has a stronger affinity for the ZSM-5 surface than water, citing the presence of the CH_3 group as a possible reason for this.[37] The CH_3OH that is retained forms coke more efficiently and lowers the mass balance of the reaction. Under higher conversion conditions the contact time with the catalyst is increased as, despite operating with a fixed bed volume, the catalyst mass is higher. Potentially, CH_3OH desorbed at the top of the catalyst bed can re-adsorb further down, reacting with Brønsted acid sites to form coke. From analysis of the delplot data we propose a reaction network (Scheme 1) whereby CO_2 formation is largely independent of CH_3OH and CO concentration, however, CO oxidation could occur. However, the stability of the CO_2 selectivity contrasts strongly against that of the CO selectivity particularly in Figure 1. The action of water to promote both CH_3OH desorption and the disproportionation of HCOOH to CO and H_2O is

captured, as proposed by Panov and co-workers.[14] Adsorption of CH_3OH at an adjacent Brønsted acid site is captured to highlight that the formation of CO and CH_3OH is unlikely to remain equivalent. The determination of CO and C_2H_4 as primary products in the delplot analysis suggests that cooperativity exists between the active Fe sites for methanol formation and Brønsted acid sites as has been suggested previously.[22] The formation of C_2H_6 is thought to occur through hydrogen transfer under the umbrella of the Methanol-to-Hydrocarbons chemistry,[34] however, we did not detect any of the expected dienes, trienes or polymethylbenzenes that would form post-transfer. We consider that this reaction would take place in the pores of the zeolite and that these products contribute to the formation of coke. Therefore, for the sake of simplicity they have been omitted from Scheme 1.

Characterisation of pre- and post-reaction samples

The delplot analysis revealed that the major reaction pathways are largely unchanged by the addition of water to the system, clarifying that the role of water is to displace methanol before it reacts further, rather than offer a different pathway. When H_2O is present, analysis of the delplot data suggests that coke can be a secondary or higher rank product (Figs. 5b and c). In addition, the deactivation rate of the catalyst was unchanged by the presence of water (Fig. 3). This was an unexpected observation as reaction data (Figs. 1 and 2) showed that the accumulation of coke/organics in the catalyst is significantly reduced when water is present, so it would be expected that this catalyst is more stable. Therefore, characterisation of the fresh and used samples from reactions in the presence and absence of water was carried out to better understand the cause of catalyst deactivation.

TGA was carried out to calculate the quantity of carbon retained after the 3 h reaction. Figure 6 illustrates the mass loss when fresh Fe-ZSM-5, Fe-ZSM-5-0% and Fe-ZSM-5-20% were heated in flowing air over the temperature range of 30 to 900 °C. The fresh catalyst and the one used with 20 % H_2O exhibit almost identical TGA profiles, with weight losses occurring below 200 °C. This is consistent with the loss of physisorbed water and carbonates. In contrast, Fe-ZSM-5-0% exhibits a broad weight loss centred at 400 °C. This is ascribed to CO_2 production, formed as coke is combusted. These observations are consistent with the poor mass balance and high selectivity to coke seen in the reaction data presented in Figure 1 and provides further evidence of the role of water in suppressing coke formation. The broad thermal event represented by a bi-modal weight loss (Fig. 6b), is consistent with observations made by Weckhuysen and co-workers[38-40] concerning coke build-up on different sites within ZSM-5.

The mass loss over the temperature range of 220 – 600 °C can be ascribed to coke formed in the reaction being removed in the form of carbon oxides, as described above. This corresponds to 795

μmol of carbon per gram of catalyst per hour ($\mu mol_C\ g_{cat}^{-1}\ h^{-1}$) for the Fe-ZSM-5-0% sample (Table 1, Entry 4). In contrast, when water was present the rate of coke accumulation was just 59 $\mu mol_C\ g_{cat}^{-1}\ h^{-1}$. The potential coking rate expressed in $\mu mol_C\ g_{cat}^{-1}\ h^{-1}$ was also calculated to compare the moles of carbon derived from TGA measurements with the expected value based on the reaction data presented in Figs. 1 and 2. Respectively, carbon deposition rates of 587 and 166 $\mu mol_C\ g_{cat}^{-1}\ h^{-1}$ were calculated for Fe-ZSM-5-0% and Fe-ZSM-5-20%, which does not match with the amount of carbon removed during the TGA analysis. A similar discrepancy was observed in the recent work of Panov and co-workers,[14] where a rate of 1400 $\mu mol_C\ g_{cat}^{-1}\ h^{-1}$ was measured by TPO, however, based on their reaction data only 795 $\mu mol_C\ g_{cat}^{-1}\ h^{-1}$ would be expected. We consider that the discrepancy observed may be due to the uneven distribution of coke along the bed profile.

The significant coking observed with Fe-ZSM-5-0% did not greatly impact the reactivity, as evidenced in Fig. 1b. The reduction of methane conversion is *ca.* 20 % over the 3 h reaction and *ca.* 40 % for N_2O (Fig. 3). The selectivity to methanol and C_2 products remains low during the time-on-line reaction, although the fall and subsequent plateau of the CO selectivity suggests that the Fe^{3+} based active sites are not all deactivated by coke. The influence of H_2O in the feed-stream was further investigated through nitrogen adsorption isotherms; these were collected for the samples and compared to the parent H-ZSM-5 material (Fig. S3). The BET surface area and micro-pore volume of the materials are shown in Table 1. As expected the addition of Fe (2 wt. %) reduced the total surface area of the parent H-ZSM-5 material by *ca.* 75 $m^2\ g^{-1}$, although the micro-pore volume was not greatly affected. Analysis of the post-reaction samples reveals that the surface area and micro-pore volume of Fe-ZSM-5-20% is comparable to that of unused, Fe-ZSM-5. This is consistent with TGA results in Fig. 6 and the relatively low carbon loss observed in Figure 2 with water in the reaction feed-stream preventing significant coke accumulation on the catalyst surface. In the case of Fe-ZSM-5-0%, the absence of water in the feed-stream has clearly affected the nitrogen adsorption measurements. The BET surface area and micro-pore volume decreased by ca. 40 % when compared to the unused Fe-ZSM-5, from 359 to 210 $m^2\ g^{-1}$ and 0.142 to 0.087 $cm^3\ g^{-1}$ respectively. These significant surface area and porosity reductions are clearly visible in the N_2 isotherm measurements displayed in Figure S3.

The formation of CO has been suggested by Panov and co-workers to originate from adsorbed CH_3OH or HCHO reacting with H_2O to HCOOH and subsequently CO.[14] Therefore, it is reasonable to expect that CH_3OH can still form via the $(Fe^{3+}\text{-}O^-)_\alpha$ site although can be retained within the zeolite pore system, potentially through surface diffusion[14, 24, 41] where water is not present. This suggests that the decreases in activity observed in Figure 1 and 2 are not strictly related to increased Fe site blocking by coke in the case of Fe-ZSM-5-0% and surface hydration in Fe-ZSM-5-20%.

UV-Vis was carried out to observe the structure of the Fe species before and after the reaction to account for the comparable N_2O decomposition rate despite differing coking rates. Figure 7 shows an overlay of spectra for Fe-ZSM-5, Fe-ZSM-5-0% and Fe-ZSM-5-20%. Bands at 210 and 240 nm correspond to the $t_1 \rightarrow t_2$ and $t_1 \rightarrow e$ transitions of the FeO_4 which are isomorphously substituted into the tetrahedral sites of the zeolite framework[42], while bands at 250 nm correspond to isolated octahedral Fe^{3+} species in extra-framework Al_2O_3.[43] Iron oxide clusters are indicated by bands at 300 to 450 nm and bulk iron oxide species are shown at $\lambda > 450$ nm.[44] Fe-ZSM-5 and Fe-ZSM-5-20% exhibit comparable spectra, whilst Fe-ZSM-5-0% exhibits more resolved bands at 210, 240, 410 and 550 - 800 nm. The latter band indicates that iron oxide clusters and bulk iron oxide on the external surface were formed during the reaction without water, and the addition of water appears to suppress this process.

The formation of Fe_xO_y clusters is common under high temperature calcination conditions[42] or through steam treatment.[45] However, the reaction temperature of 300 °C is not considered sufficient to promote Fe migration, as this typically occurs >600 °C and is favoured by high heating rate. The formation of Fe_xO_y clusters is also more likely to occur when moisture remained in the zeolite as observed by Kumar *et al*.[42] Therefore, the formation of the distinct iron oxide clusters observed in the Fe-ZSM-5-0% sample is intriguing. The rapid accumulation of coke that occurs may be linked to the instability of the Fe^{3+} active sites in the absence of water. Reductive treatment of Fe^{3+} in FeZSM-5 is known to result in an irreversible agglomeration process forming Fe_3O_4. This Fe_3O_4 magnetite phase can readily undergo further transformation to α-Fe_2O_3 particles by subsequent oxidation[46], which may be represented by the broad band observed from 550 to 800 nm. Furthermore, this broad band signifies the irreversible redistribution of Fe ion species following treatment with CH_4 and N_2O. The redox properties of the isolated Fe^{3+} ions may also be different when coexisting with a large concentration of Fe_xO_y clusters, as observed with NO reduction in a previous report.[42] We consider that weakly bound Fe^{3+} may migrate when water is not present to yield iron oxide species, however, as the conversion of methane and N_2O remain stable after 100 min time-on-line (Fig. 1). Such migration appears to be unrelated to the activity of the catalyst. According to the UV/Vis spectra, Fe-ZSM-5-0% has retained a sufficient quantity of FeO_4 tetrahedra and extra-framework Fe to complete the methane oxidation reaction via the α-oxygen species.

In order to further investigate the origin of Fe restructuring and catalyst deactivation, control experiments with 20% CH_4/Ar or 2% N_2O/Ar were fed over the catalyst at 300 °C for 3 h and UV-Vis spectroscopy was carried out on the used catalysts (Fig. 8). It can be seen that the spectra are very similar after the control experiments were carried out, indicating that the Fe speciation did not greatly change as a result of exposure to N_2O or CH_4. However, in both samples exposed to CH_4 or N_2O there

were modest shifts to higher wavelengths. This implies that a modest restructuring of Fe can occur with CH_4 or N_2O present, however, the cause of the significant shifts seen in Fe-ZSM-5-0% could be due to an intermediate or reaction product that was not present in these control experiments.

Additionally, the stability of N_2O conversion in the absence of CH_4 was examined to determine if the catalyst deactivation observed was related to poisoning of the active site induced by N_2O (Fig. 9). A control experiment was carried out which involved passing 2 % N_2O in Ar over the Fe-ZSM-5 catalyst. The conversion of N_2O was normalised to the initial value (after 5 min on-stream) and compared in Figure 9. This is plotted with N_2O conversion rates from the methane oxidation reactions which were presented in Figure 3. The N_2O conversion rate dropped rapidly in the control experiment, but was slightly more stable than the full reaction feed. In the absence of a reductant, N_2O decomposition is rate-limited at lower temperatures, such as 300 °C, by oxygen recombination.[47] Specifically, the dissociation of N_2O on Fe sites is facile, but the reaction does not turn over because O_2 must be formed from two oxygen atoms to close the catalytic cycle. We consider that the rapid drop in N_2O conversion observed in Figure 9 could be due to saturation of -Fe^{2+} sites by N_2O and that the rate of CH_4 activation is lower than that of N_2O dissociation. The decrease in N_2O turn-over appears to be a limiting factor to efficient CH_4 conversion and appears unaffected by Fe restructuring or coke accumulation.

Overall, the characterisation of the fresh and used catalyst showed that the introduction of water suppressed coke formation, by promoting the desorption of methanol from the surface. Additionally, it was found that in the absence of water, the Fe species restructured during the reaction. However, the overall rate of catalyst deactivation was the same with and without water present, suggesting that these processes were not affecting the catalytic turnover of CH_4. Thermal-gravimetric analysis and N_2 porosimetry revealed coke formation and surface area loss during reactions carried out in the absence of water. Therefore, it is possible that the deactivation of the catalyst in the absence of water is caused by coke formation near $(Fe^{3+}\text{-}O^{-})_{\alpha}$, loss of porosity and Fe restructuring. Additionally, the initial drop in N_2O conversion rates results from slow regeneration of these species. Interestingly, a similar rate of deactivation occurs when water, a known inhibitor of N_2O decomposition, is present.[48]

Conclusion

The influence of water on the reaction of CH_4 and N_2O over Fe-ZSM-5 catalysts was probed with delplot analysis. The yield of methanol on *alpha*-oxygen sites $(Fe^{3+}\text{-}O^{-})_{\alpha}$ is low, particularly under the reaction conditions studied, as the rate of CH_3OH desorption is low on Fe-ZSM-5 catalysts.[14] In the absence of water, CH_3OH can migrate to nearby Brønsted acid sites where it is converted to coke via processes exemplified in the MTO reaction.[30, 31] Indeed, delplot analysis showed that coke is a secondary reaction product when water is not present. Conversely, in the presence of water, coke becomes a secondary or tertiary product, indicative of a reduction in the rate of formation of coke. Other reaction products including CO and C_2H_4 were found to be primary products, which further implies slow desorption of CH_3OH or a methoxy species from the catalyst surface. Interestingly, with increasing methane conversion, CO_2 selectivity was found to be largely independent of variations in the yield of coke or CO. This suggested that total oxidation of methane or other oxygenates operates via a separate pathway and is not influenced by the presence of water. Furthermore, characterisation studies show that water can prevent loss of catalyst porosity through inhibiting coke formation, whilst also preventing migration/ aggregation of Fe species. Therefore, the complex reaction mechanism of selective methane oxidation appears to be greatly affected by the presence of water and the decomposition rate of N_2O. It is clear that catalyst deactivation occurs at a rate which is unaffected by water addition, suggesting that coking and changes in iron speciation do not have a significant detrimental effect upon catalyst performance at the short reaction times on stream studied. In the absence of CH_4, the rate of N_2O conversion also decreased rapidly, suggesting a common mechanism of deactivation which is independent of catalyst fouling. This investigation clarifies the reaction pathway of methane activation using N_2O over Fe-ZSM-5 and underlines the complex nature of the reaction, where multiple reaction and deactivation pathways take place.

Acknowledgments

The authors wish to thank ExxonMobil for financial support.

References

[1] A. I. Olivos-Suarez, A. Szecsenyi, E. J. M. Hensen, J. Ruiz-Martinez, E. A. Pidko, J. Gascon *Acs Catalysis*. **2016**, 6, 2965-2981.
[2] M. J. da Silva *Fuel Processing Technology*. **2016**, 145, 42-61.
[3] G. A. Olah *Angewandte Chemie-International Edition*. **2005**, 44, 2636-2639.
[4] T. Mokrani, M. Scurrell *Catalysis Reviews-Science and Engineering*. **2009**, 51, 1-145.
[5] C. Hammond, M. M. Forde, M. H. Ab Rahim, A. Thetford, Q. He, R. L. Jenkins, N. Dimitratos, J. A. Lopez-Sanchez, N. F. Dummer, D. M. Murphy, A. F. Carley, S. H. Taylor, D. J. Willock, E. E. Stangland, J. Kang, H. Hagen, C. J. Kiely, G. J. Hutchings *Angewandte Chemie-International Edition*. **2012**, 51, 5129-5133.
[6] J. A. Labinger *Journal of Molecular Catalysis a-Chemical*. **2004**, 220, 27-35.
[7] K. Narsimhan, K. Iyoki, K. Dinh, Y. Roman-Leshkov *Acs Central Science*. **2016**, 2, 424-429.
[8] V. S. Arutyunov *Journal of Natural Gas Chemistry*. **2004**, 13, 10-22.
[9] M. H. Groothaert, P. J. Smeets, B. F. Sels, P. A. Jacobs, R. A. Schoonheydt *Journal of the American Chemical Society*. **2005**, 127, 1394-1395.
[10] P. J. Smeets, M. H. Groothaert, R. A. Schoonheydt *Catalysis Today*. **2005**, 110, 303-309.
[11] P. Tomkins, A. Mansouri, S. E. Bozbag, F. Krumeich, M. B. Park, E. M. C. Alayon, M. Ranocchiari, J. A. van Bokhoven *Angewandte Chemie-International Edition*. **2016**, 55, 5467-5471.
[12] V. L. Sushkevich, D. Palagin, M. Ranocchiari, J. A. van Bokhoven *Science*. **2017**, 356, 523-+.
[13] J. Xu, R. D. Armstrong, G. Shaw, N. F. Dummer, S. J. Freakley, S. H. Taylor, G. J. Hutchings *Catalysis Today*. **2016**, 270, 93-100.
[14] M. V. Parfenov, E. V. Starokon, L. V. Pirutko, G. I. Panov *Journal of Catalysis*. **2014**, 318, 14-21.
[15] G. I. Panov, E. V. Starokon, L. V. Pirutko, E. A. Paukshtis, V. N. Parmon *Journal of Catalysis*. **2008**, 254, 110-120.
[16] B. R. Wood, J. A. Reimer, A. T. Bell, M. T. Janicke, K. C. Ott *Journal of Catalysis*. **2004**, 225, 300-306.
[17] M. C. Kung, S. S. Y. Lin, H. H. Kung *Topics in Catalysis*. **2012**, 55, 108-115.
[18] D. A. Bulushev, P. M. Prechtl, A. Renken, L. Kiwi-Minsker *Industrial & Engineering Chemistry Research*. **2007**, 46, 4178-4185.
[19] N. A. Bhore, M. T. Klein, K. B. Bischoff *Industrial & Engineering Chemistry Research*. **1990**, 29, 313-316.
[20] H. J. Wei, C. Gomez, J. J. Liu, N. Guo, T. P. Wu, R. Lobo-Lapidus, C. L. Marshall, J. T. Miller, R. J. Meyer *Journal of Catalysis*. **2013**, 298, 18-26.
[21] T. Rajkhowa, G. B. Marin, J. W. Thybaut *Applied Catalysis B: Environmental*. **2017**, 205, 469-480.
[22] K. Chow, N. F. Dummer, J. Carter, C. Williams, G. Shaw, D. J. Willock, S. H. Taylor, S. Yacob, R. J. Meyer, M. Bhasin, G. J. Hutchings *Catalysis Science & Technology*. **2017**.
[23] G. I. Panov, K. A. Dubkov, E. V. Starokon *Catalysis Today*. **2006**, 117, 148-155.
[24] E. V. Starokon, M. V. Parfenov, S. S. Arzumanov, L. V. Pirutko, A. G. Stepanov, G. I. Panov *Journal of Catalysis*. **2013**, 300, 47-54.
[25] E. V. Starokon, M. V. Parfenov, L. V. Pirutko, S. I. Abornev, G. I. Panov *Journal of Physical Chemistry C*. **2011**, 115, 2155-2161.
[26] G. N. Li, E. A. Pidko, R. A. van Santen, Z. C. Feng, C. Li, E. J. M. Hensen *Journal of Catalysis*. **2011**, 284, 194-206.

[27] K. A. Dubkov, N. S. Ovanesyan, A. A. Shteinman, E. V. Starokon, G. I. Panov *Journal of Catalysis*. **2002**, 207, 341-352.
[28] M. F. Fellah, I. Onal *Journal of Physical Chemistry C*. **2010**, 114, 3042-3051.
[29] B. E. R. Snyder, P. Vanelderen, M. L. Bols, S. D. Hallaert, L. H. Bottger, L. Ungur, K. Pierloot, R. A. Schoonheydt, B. F. Sels, E. I. Solomon *Nature (London, U. K.)*. **2016**, 536, 317-321.
[30] P. Tian, Y. X. Wei, M. Ye, Z. M. Liu *Acs Catalysis*. **2015**, 5, 1922-1938.
[31] M. Z. Zhang, S. T. Xu, Y. X. Wei, J. Z. Li, J. R. Chen, J. B. Wang, W. N. Zhang, S. S. Gao, X. J. Li, C. X. Wang, Z. M. Liu *Rsc Advances*. **2016**, 6, 95855-95864.
[32] K. Chen, J. Damron, C. Pearson, D. Resasco, L. Zhang, J. L. White *ACS Catalysis*. **2014**, 4, 3039-3044.
[33] M. Bjorgen, S. Svelle, F. Joensen, J. Nerlov, S. Kolboe, F. Bonino, L. Palumbo, S. Bordiga, U. Olsbye *Journal of Catalysis*. **2007**, 249, 195-207.
[34] S. Ilias, A. Bhan *ACS Catalysis*. **2013**, 3, 18-31.
[35] G. I. Panov, K. A. Dubkov, Y. A. Paukshtis *Catalysis by Unique Metal Ion Structures in Solid Matrices: from Science to Application*. **2001**, 13, 149-163.
[36] S. Svelle, F. Joensen, J. Nerlov, U. Olsbye, K. P. Lillerud, S. Kolboe, M. Bjorgen *Journal of the American Chemical Society*. **2006**, 128, 14770-14771.
[37] B. Hunger, S. Matysik, M. Heuchel, W.-D. Einicke *Langmuir*. **1997**, 13, 6249-6254.
[38] D. Mores, E. Stavitski, M. H. F. Kox, J. Kornatowski, U. Olsbye, B. M. Weckhuysen *Chemistry-a European Journal*. **2008**, 14, 11320-11327.
[39] D. Mores, J. Kornatowski, U. Olsbye, B. M. Weckhuysen *Chemistry-a European Journal*. **2011**, 17, 2874-2884.
[40] L. R. Aramburo, S. Teketel, S. Svelle, S. R. Bare, B. Arstad, H. W. Zandbergen, U. Olsbye, F. M. F. de Groot, B. M. Weckhuysen *Journal of Catalysis*. **2013**, 307, 185-193.
[41] G. K. Boreskov in *Catalytic Activation of Dioxygen, Vol.*, Springer Berlin Heidelberg, Berlin, Heidelberg, **1982**, pp.39-137.
[42] M. S. Kumar, M. Schwidder, W. Grünert, A. Brückner. **2004**, 227, 384-397.
[43] M. Schwidder, W. Grunert, U. Bentrup, A. Bruckner *Journal of Catalysis*. **2006**, 239, 173-186.
[44] J. Perez-Ramirez, M. S. Kumar, A. Bruckner *Journal of Catalysis*. **2004**, 223, 13-27.
[45] H. T. Lee, H. K. Rhee *Korean Journal of Chemical Engineering*. **2002**, 19, 574-579.
[46] A. V. Kucherov, C. N. Montreuil, T. N. Kucherova, M. Shelef *Catalysis Letters*. **1998**, 56, 173-181.
[47] L. Kiwi-Minsker, D. A. Bulushev, A. Renken *Catalysis Today*. **2005**, 110, 191-198.
[48] D. A. Bulushev, L. Kiwi-Minsker, A. Renken *Journal of Catalysis*. **2004**, 222, 389-396.

Tables, Schemes and Figures

Table 1. BET surface areas and pore volumes of MFI catalysts pre- and post-reaction.

Entry	Catalyst	Total surface area[a, b] ($m^2\ g^{-1}$)	$V_{micropore}$[b] ($cm^3\ g^{-1}$)	Coke produced[c] ($\mu mol_C\ g_{cat}^{-1}\ h^{-1}$)	Missing carbon[d] ($\mu mol_C\ g_{cat}^{-1}\ h^{-1}$)
1	H-ZSM-5	434	0.169	-	-
2	Fe-ZSM-5	359	0.142	-	-
3	Fe-ZSM-5-20%	352	0.134	59	166
4	Fe-ZSM-5-0%	210	0.087	795	587

[a] Surface area determined from nitrogen adsorption measurement using the BET equation at -196 °C. [b] Quantitative analysis is per unit mass of sample – in the case of Entry 4 this includes *ca*. 5 wt. % carbonaceous deposits. [c] Coke production calculated from mass loss over 200 – 600 °C from TGA measeurements as described in experimental section. [d] Expected missing carbon calculated from yield of missing carbon from 3 h time on-stream tests presented in Figs. 1 and 2.

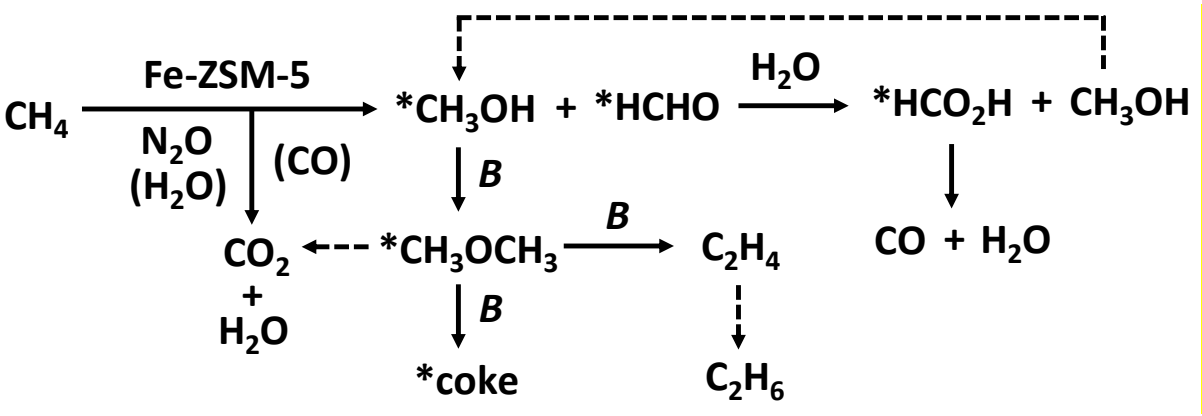

Scheme 1. Proposed reaction network for CH_4 oxidation with N_2O over Fe-ZSM-5 catalysts according to delplot analysis; ***B*** is Brønsted acid site and * indicates adsorbed or intermediate species not detected in the reactor effluent.

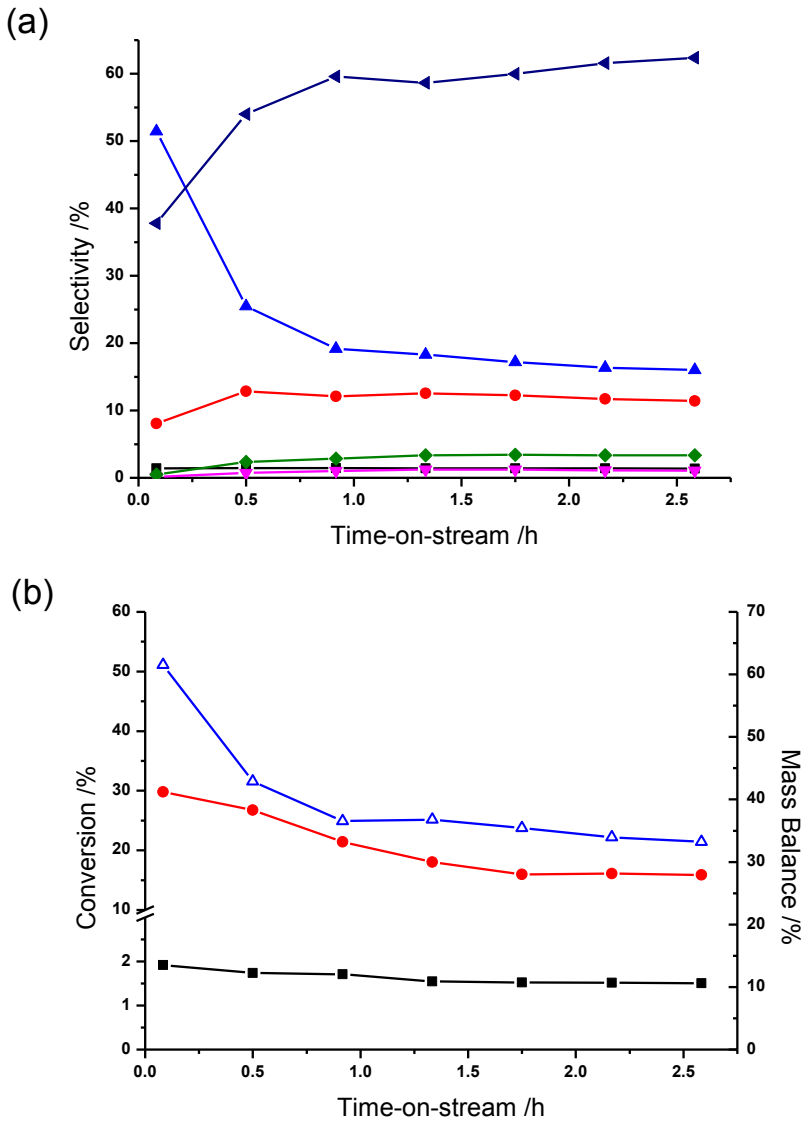

Fig. 1. The oxidation of methane over 2 % Fe/ZSM-5 (30) using N_2O at 300 °C showing (a) temporal evolution of products (▲ CO; ■ CH_3OH; ● CO_2; ◆C_2H_6; ▼C_2H_4 and ◀ ''missing carbon'') and (b) carbon mass balance (△) and conversion of methane (■)/N_2O (●).

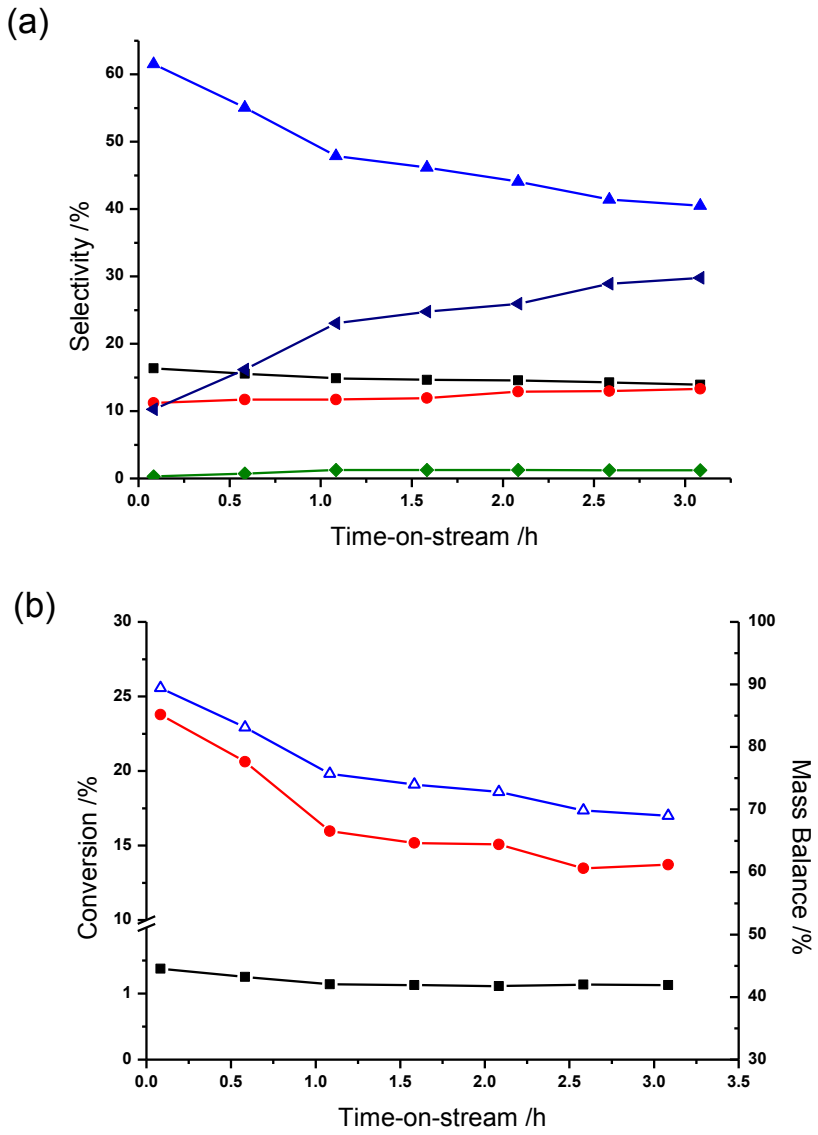

Fig. 2. The oxidation of methane over 2.5 % Fe/ZSM-5 (30) using N_2O at 300 °C with 20 % v/v H_2O added to the substrate feed, showing (a) temporal evolution of products (▲ CO; ■ CH_3OH; ● CO_2; ◆C_2H_6 and ◀ ''missing carbon'') and (b) carbon mass balance (△) and conversion of methane (■)/N_2O (●).

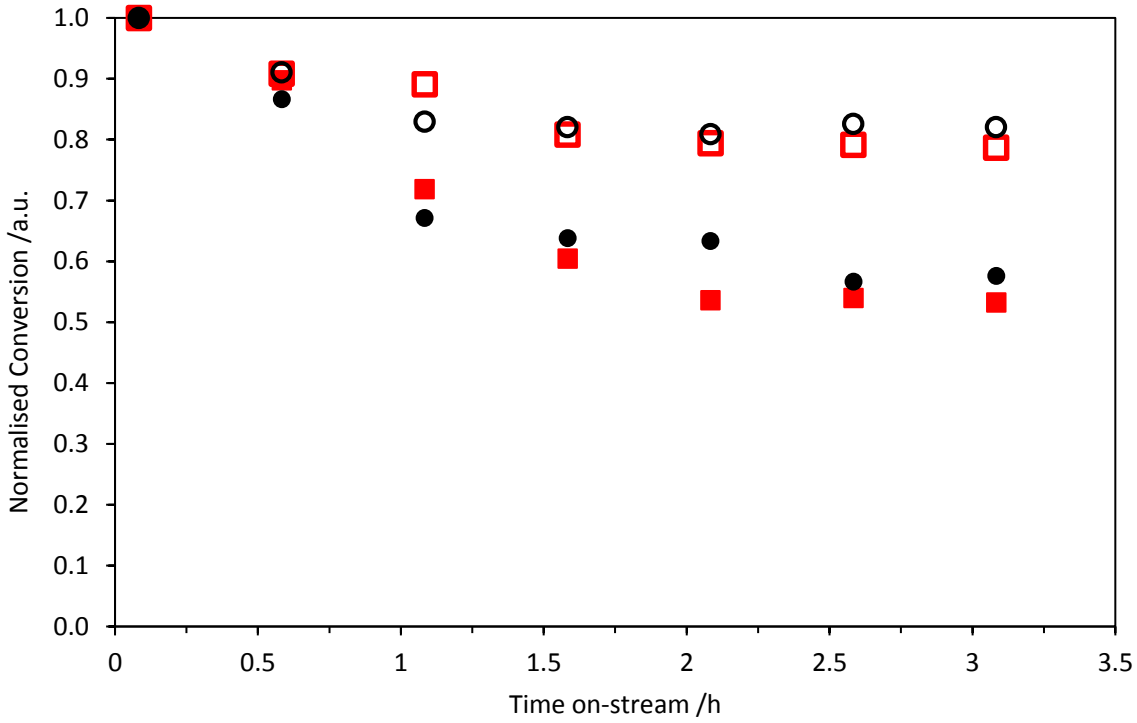

Fig. 3. The conversion of methane (20 % H_2O ■ and 0 % H_2O ●) and N_2O (20 % H_2O □ and 0 % H_2O ○) normalised to their initial values at t_5 over 2% Fe/ZSM-5 at 300 °C.

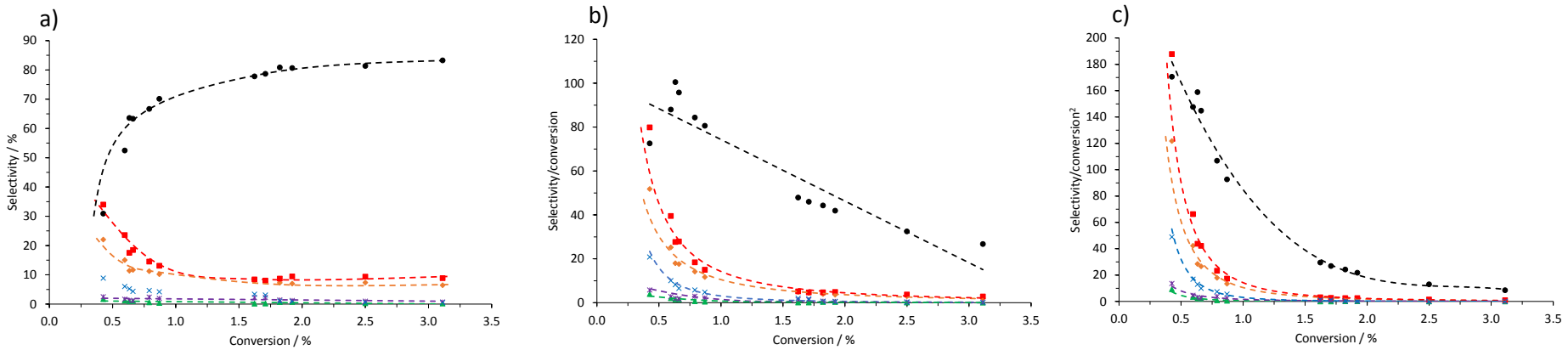

Fig. 4. First rank (a), second rank (b) and third rank (c) delplots taken from data collected over a series of experiments using different masses of 2 % Fe-ZSM-5 at 300 °C; (▲) CH_3OH, (◆) CO_2, (■) CO, (∗) C_2H_6, (✕) C_2H_4 and (●) missing carbon.

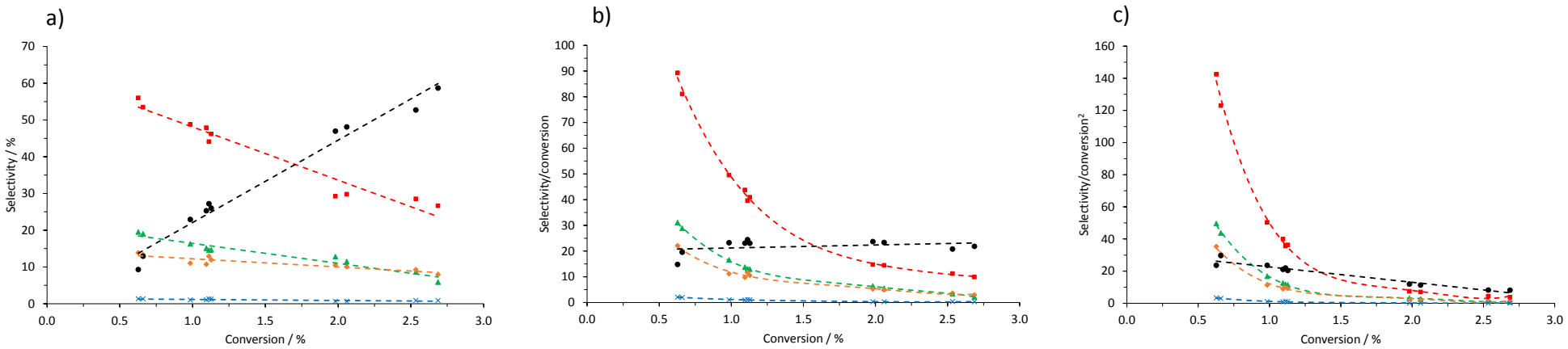

Fig. 5. First rank (a), second rank (b) and third rank (c) delplots taken from data collected over a series of experiments using varying masses of 2 % Fe-ZSM-5 at 300 °C with water present in the feed-stream; (▲) CH_3OH, (◆) CO_2, (■) CO, (✕) C_2H_4 and (●) missing carbon.

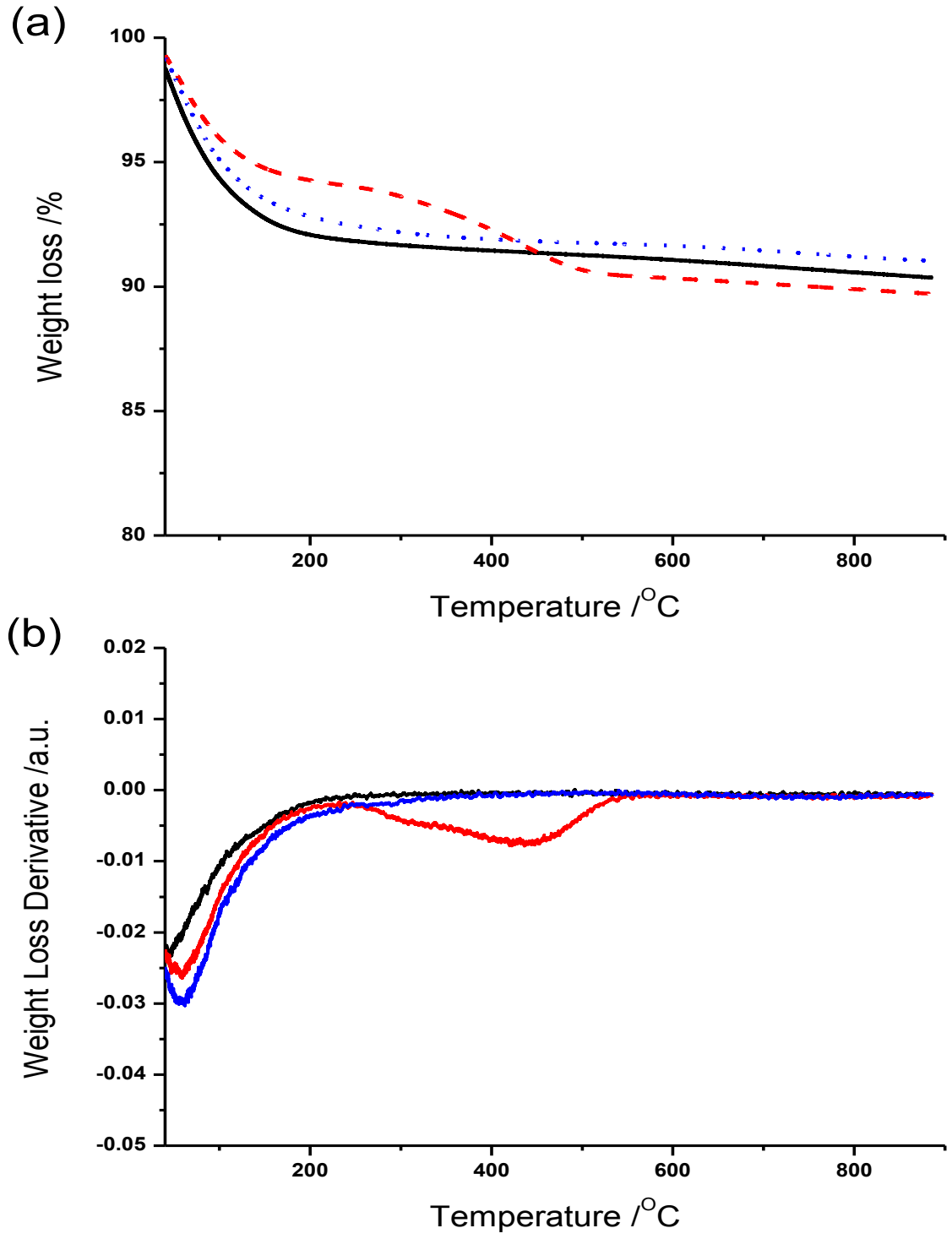

Fig. 6. TGA profiles of fresh and used catalysts showing weight loss profiles (a) and weight loss derivate profiles (b) for Fe-ZSM-5 (black), Fe-ZSM-5-20% (blue dots) and Fe-ZSM-5-0% (red dashes).

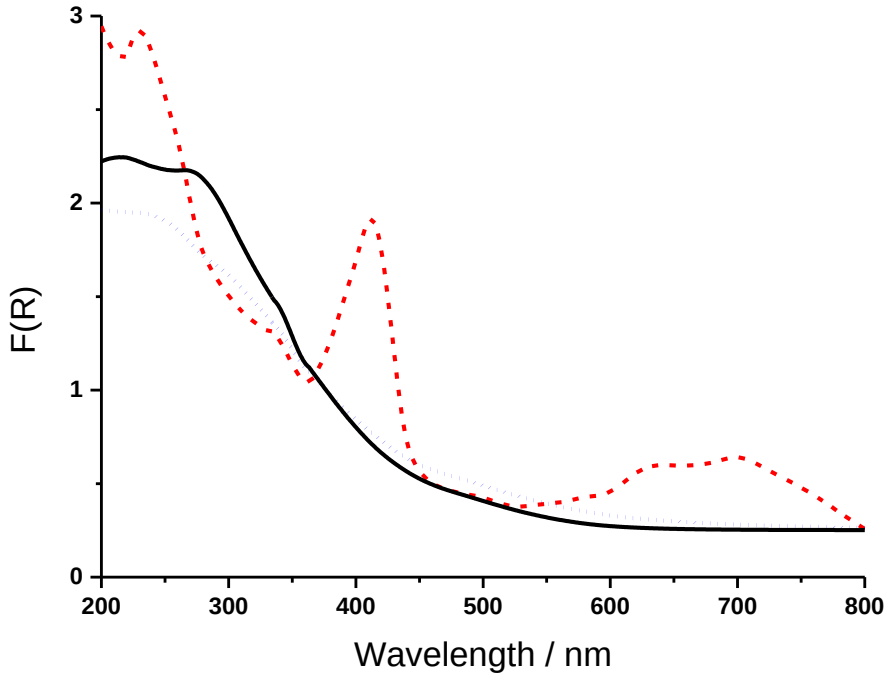

Fig. 7. UV-vis spectra of Fe-ZSM-5 (black line), Fe-ZSM-5-20% (blue dots) and Fe-ZSM-5-0% (red dashes).

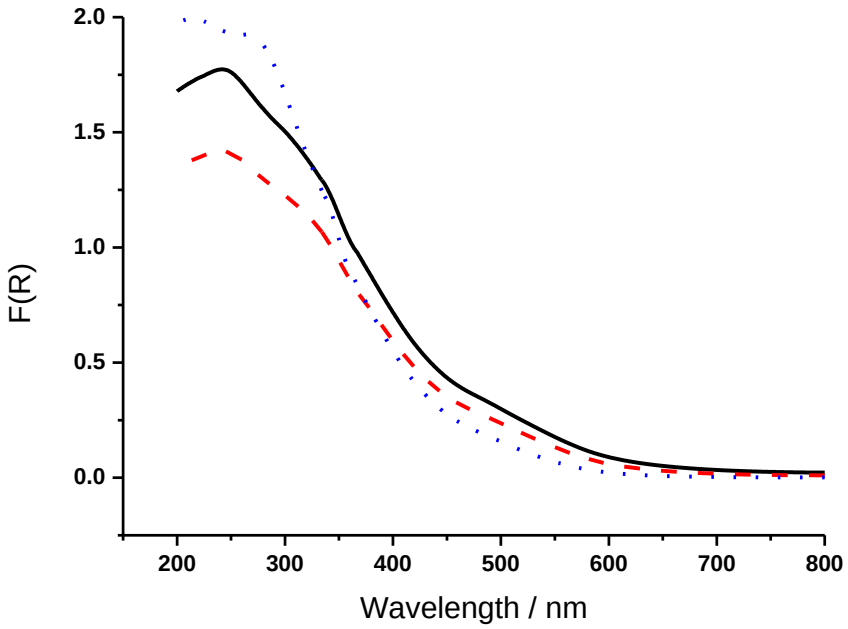

Fig. 8. UV-Vis spectra of fresh 2 % Fe-ZSM-5 (blue dots) and following control experiments under 20% CH_4/Ar (black line) and 2% N_2O/Ar (red dashes).

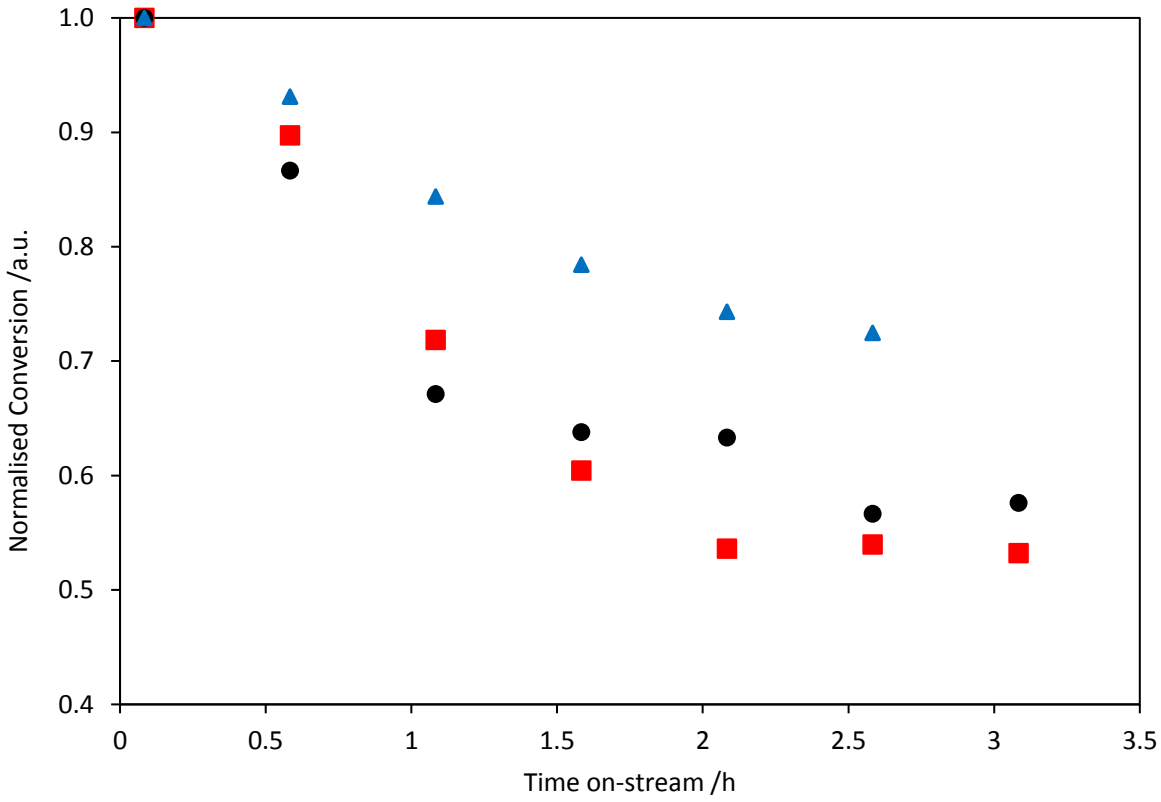

Fig. 9. Normalised N_2O conversion over 2% Fe/ZSM-5 at 300 °C in flows of; CH_4 + 2% N_2O (●), 20% CH_4 + 2% N_2O + 20% H_2O (■) and 2% N_2O (▲) at 300 °C over 2 wt.% Fe-ZSM-5 normalised to their initial values. All gas compositions balanced with Ar. Total flow rate = 55 ml min^{-1}.